

PACS numbers: 81.05.Uw; 33.80.Rm; 42.65.Re
DOI: 10.1070/QE2014v044n12ABEH015459

Propagation and absorption of high-intensity femtosecond laser radiation in diamond

V.V. Kononenko, V.I. Konov, V.M. Gololobov, E.V. Zavedeev

Abstract. **Femtosecond interferometry has been used to experimentally study the photoexcitation of the electron subsystem of diamond exposed to femtosecond laser pulses of intensity 10^{11} to 10^{14} W cm^{-2}. The carrier concentration has been determined as a function of incident intensity for three harmonics of a Ti:sapphire laser (800, 400 and 266 nm). The results demonstrate that, in a wide range of laser fluences (up to those resulting in surface and bulk graphitisation), a well-defined multiphoton absorption prevails. We have estimated nonlinear absorption coefficients for pulsed radiation at λ = 800 nm (four-photon transition) and at 400 and 266 nm (indirect and direct two-photon transitions, respectively). It has also been shown that, at any considerable path length of a femtosecond pulse in diamond (tens of microns or longer), the laser beam experiences a severe nonlinear transformation, determining the amount of energy absorbed by the lattice, which is important for the development of technology for diamond photostructuring by ultrashort pulses. The competition between wave packet self-focusing and the plasma defocusing effect is examined as a major mechanism governing the propagation of intense laser pulses in diamond.**

Keywords: *femtosecond laser radiation, diamond, multiphoton absorption, nonlinear propagation, femtosecond interferometry.*

1. Introduction

Laser modification of the structure of transparent solids is a convenient and flexible tool for producing local changes in their optical and physical properties [1, 2]. To successfully employ such technologies, one should, first of all, ensure close control over the process. In this context, photomodification is a very attractive approach. Its principle is that, when excited carriers relax, the excitation energy is transferred to the lattice, heating it or producing point defects [3]. Basically, each of these effects, governed by its own internal mechanisms, leads to permanent structural changes in the zone under irradiation, which become more pronounced with each pulse. Nevertheless, it is clear that the photomodification process is difficult to control in this stage. The amount of electron–hole (e–h) pairs generated in the material is much easier to control.

In the case of single- or two-photon absorption, this is a relatively trivial issue, and the degree of modification usually depends only on laser fluence [4]. A serious drawback to this approach is that the possibility of local optical energy deposition in the bulk of a material is inherently limited, whereas most interest is currently focused on three-dimensional (3D) modification of transparent materials. A viable alternative is to employ high-intensity light at a relatively low (below-band-gap) photon energy. In this approach, at a sufficient degree of absorption nonlinearity, free carriers can be generated in the vicinity of the focal region, almost without exciting the electron subsystem outside it. For this reason, since the first experimental demonstration of fused silica densification by femtosecond laser radiation [5], this approach has been the subject of intense research, with application not only to silicate glasses but also to a variety of wide-band-gap dielectrics, including diamond [6].

Nevertheless, it should be emphasised that, in the case of strong nonlinearity, light–matter interaction has inherent features that do not always help to control the laser modification process. In our opinion, two aspects are critical. First, nonlinearity should not have an explosive character, which otherwise might lead to appreciable contributions of inverse bremsstrahlung and electron impact-induced transitions. This may be accompanied by an avalanche, which typically results in macroscopic damage to the material. Thus, the light absorption mechanism depends on particular material subjected to femtosecond photomodification.

The other critical aspect is related to the necessity of ensuring high carrier concentration. To this end, intensities from 10^{12} to 10^{14} W cm^{-2} are needed, depending on the material. For the vast majority of dielectrics, the Kerr effect is important under such conditions. As a result, the competition between laser beam self-focusing and the defocusing effect of the plasma plume may lead to severe distortion of the wavefront, an energy redistribution in the beam and, as a consequence, to unpredictable changes in photogenerated carrier concentration.

In this paper, we report an experimental study of the above aspects of the effect of femtosecond laser radiation on single-crystal diamond. This research was prompted by recent results on 3D microstructuring of diamond [7]. Despite the significant practical advances in 3D diamond graphitisation by ultrashort laser pulses, experimental data on the mechanisms of nonlinear absorption in diamond at pulse intensities sufficient for its graphitisation are limited to the UV spectral region [8] and nonlinear transformations of the beam under such conditions are essentially unexplored.

V.V. Kononenko, V.I. Konov, E.V. Zavedeev A.M. Prokhorov General Physics Institute, Russian Academy of Sciences, ul. Vavilova 38, 119991 Moscow, Russia; National Nuclear Research University MEPhI, Kashirskoe shosse 31, 115409 Moscow, Russia; e-mail: kononenko@nsc.gpi.ru;
V.M. Gololobov A.M. Prokhorov General Physics Institute, Russian Academy of Sciences, ul. Vavilova 38, 119991 Moscow, Russia;

Received 3 March 2014; revision received 23 October 2014
Kvantovaya Elektronika **44** (12) 1099–1103 (2014)
Translated by O.M. Tsarev

2. Experimental

The laser system included a Ti:sapphire oscillator (Tsunami, Spectra Physics) and a regenerative amplifier (Spitfire, Spectra Physics) operating at 800 nm (Fig. 1). The diamond single crystal used in our experiments was grown by plasma CVD and was mechanically polished on four faces. To prevent self-focusing before the geometric focus, after frequency conversion the laser beam was focused onto one of the faces of the crystal by an $f = 35$ mm spherical lens.

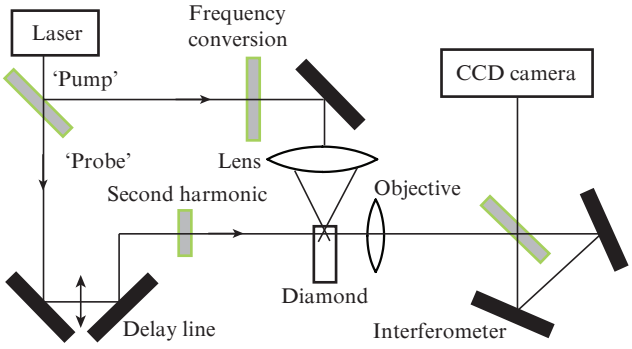

Figure 1. Schematic of the experimental setup.

To visualise the irradiation results, we used the pump–probe technique (Fig. 1). After a beam splitter, the probe beam passed through a delay line and frequency doubler and impinged on the lateral surface of the crystal. The image of the region exposed to the high-intensity laser light was projected onto the plane of a CCD camera at a magnification of 30×, digitised and processed.

A key method for gaining quantitative information about the state of the material during and after laser irradiation was femtosecond interferometry [9]. A Sagnac interferometer was placed between a projection objective lens and the CCD camera. The interference pattern observed on a display was produced by two beams, both having a local phase disturbance due to the change in the index of refraction, n, in the irradiated region. Since the interference fringes were rather broad, their shift in the irradiated region led to local changes in image brightness, which allowed us to observe and evaluate the change in n using the inverse Abel transformation. Thus, we obtained two, fundamentally identical images (negative and positive) of the affected region. One of them is presented in Fig. 2. Varying the time delay of the probe beam under fixed irradiation conditions, we obtained a series of such images, which allowed us to follow the dynamics of the disturbance and relaxation of the medium at any point of the laser caustic. The estimated error of Δn determination was within 20%. The measurement procedure was described in greater detail elsewhere [10, 11].

3. Results and discussion

The measurement procedure used allows one to follow the photoinduced disturbance of the electron subsystem of the medium by measuring the laser pulse-induced polarisation of the material. When transparent solids are exposed to intense pulses, two channels of such polarisation prevail.

One of them is the optical Kerr effect. In diamond, this effect is due to the deformation of its electron orbitals and causes the polarisability of the medium to increase with increasing field intensity: $n = n_0 + n_2 I$. The Kerr coefficient of diamond is $n_2 \approx 2 \times 10^{-15}$ cm^2 W^{-1} ($\lambda = 407$ nm) [12], which allows the Kerr response to be detected with our experimental setup at laser pulse intensities above 10^{11} W cm^{-2}. Since the effect is very fast, hyperpolarisation of the material occurs only in the presence of a field, thus producing an 'image' of a laser pulse propagating through the material (Fig. 2). It is extremely important that the photoinduced index change Δn can be measured at any point of the laser caustic, providing information about the local field intensity during femtosecond pulse propagation, i.e. when there is a strong nonlinear absorption, scattering and self-focusing.

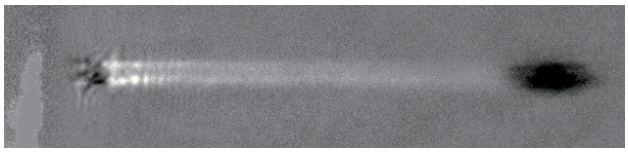

Figure 2. Interference image illustrating the propagation of a femtosecond pulse (from left to right) in diamond (266 nm, 120 fs, 90 nJ). One can see the surface of the sample (at left), the wave packet proper (black) and the plasma channel (white). The horizontal size of the image is 300 μm.

The other induced polarisation source is photoinduced transitions and electron–hole plasma formation. Free carrier generation leads to a proportional decrease in n, which can be described in terms of the classical concepts of Drude theory: $\Delta n = -(2\pi e^2)/(n_0 \omega^2 m) N_e$, where n_0 is the refractive index; ω is the laser frequency; $m = 0.5 m_e$ is the optical carrier effective mass; N_e is the carrier concentration; and e and m_e are the charge and mass of an electron. Like in the case of electric field assessment from Kerr hyperpolarisation, the e–h plasma density can be measured at any point of the laser caustic.

The plasma component of Δn was determined ~500 fs after pulse propagation through a point of observation. It should, however, be noted that the Kerr component is rather difficult to properly measure. Since Kerr hyperpolarisation and ionisation of a crystal occur simultaneously, the photoinduced change in n generally produces a rather complex picture in the interference image, so that it may prove impossible to separately assess the $+\Delta n$ and $-\Delta n$ variable contributions. In our experiments, however, even at the highest energy density, which did not exceed 10 J cm^{-2}, the plasma contribution to Δn was relatively small, disturbing for the most part the pulse 'trail'. This allowed the positive part of Δn at the instant when the pulse peak passed through the point of observation to be assessed with reasonable accuracy. According to our estimates, the accuracy was 20% or better.

Figures 3, 4 and 6 plot the free electron concentration (N_e) and the energy density in a wave packet (E_b) in a sample against laser fluence on the sample surface (E_s). E_s was evaluated from the measured laser pulse energy, and N_e and E_b were calculated from Δn. For all harmonics, the measurements were performed at two points on the optical axis. One point was located in a fixed position as close as possible to the surface (~50 μm) in order to minimise the beam path length in the crystal and, hence, reduce the nonlinear distortion of

the beam. The position of the other point was varied along the beam axis and corresponded to the maximum in N_e, i.e. to the centre of the plasma plume. Depending on irradiation conditions, this point might coincide with the former point or be up to 500 μm away from the surface. Measurements at this point were intended to characterise the distortion of the wavefront. Figures 3–5 indicate E_c: the energy density corresponding to the critical power under the focusing conditions of this study.

The $N_e(E_s)$ and $E_b(E_s)$ data for the fundamental harmonic (λ = 800 nm) are presented in Fig. 3. It is seen that the laser fluence in the sample near its surface is proportional to the incident laser fluence, i.e. the energy loss due to nonlinear absorption is relatively small. Thus, if the path length of a femtosecond pulse in diamond does not exceed a few tens of microns, possible nonlinear distortions of its wavefront do not have time to cause any field redistribution in the beam. The carrier concentration vs. E_s then shows an almost power-law behaviour, with an exponent of 4. The power-law behaviour of $N_e(E_s)$ indicates that, in a wide range of laser fluences (up to the ablation threshold, ~3 J cm^{-2}), carrier generation is only due to four-photon absorption, and not to any other process.

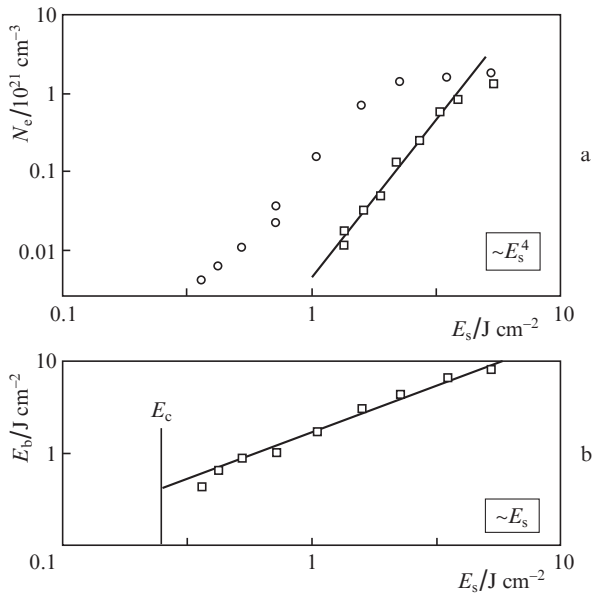

Figure 3. (a) Concentration of e–h pairs in a diamond single crystal [here and in the following figures: at the maximum in electron concentration (○) and just below the crystal surface (□)] and (b) laser fluence inside the crystal vs. laser fluence on the crystal surface (λ = 800 nm).

Note, however, that the density of the e–h plasma forming near the surface was not the highest at a fixed irradiation intensity. Since the incident power considerably exceeded the critical power (Fig. 3), a laser pulse experienced strong self-focusing when propagating through the material. At an incident laser fluence of ~1 J cm^{-2}, the beam diameter decreased from 6 to 4 μm at a depth of ~500 μm. Note that, at a given E_s, the photoinduced plasma density in the bulk of the crystal was higher than that near the surface by more than one order of magnitude, and N_e was a rather intricate function of E_s (Fig. 3).

Similar results were obtained when diamond was exposed to femtosecond pulses at λ = 400 nm (Fig. 4). For E_s < 1 J cm^{-2}, E_b is a linear function of E_s. At higher laser fluences, it saturates, which means losses, presumably dominated by two-photon absorption, but plasma defocusing also cannot be ruled out. The carrier concentration measured near the surface varies almost quadratically with laser fluence. The maximum e–h pair concentration at $E_s < E_{th} \approx 0.4$ J cm^{-2} behaves as in the above case of irradiation at λ = 800 nm. If the laser fluence exceeds E_{th}, the light does not reach the bulk of the sample. As a result, plasma is generated predominantly near the surface (at a depth of several tens of microns) and the $N_e(E_s)$ curves for $E_s > E_{th}$ coincide.

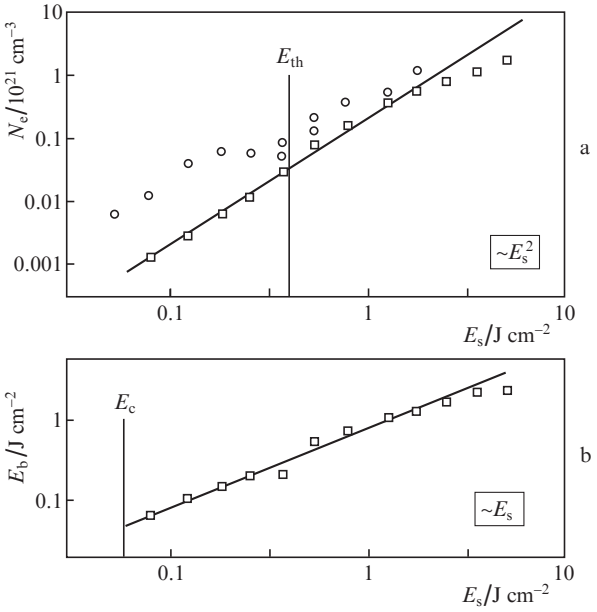

Figure 4. (a) Concentration of e–h pairs in a diamond single crystal and (b) laser fluence inside the crystal vs. laser fluence on the crystal surface (λ = 400 nm).

This effect is rather important from the viewpoint of practical application. Control over the excited carrier concentration and, hence, over the energy transferred to the lattice is a nontrivial issue in spite of the well-known absorption value. This is obviously due to the severe transformation of a Gaussian beam in the material at the intensities in question.

The nature of pulse propagation was uniquely determined by the competition between self-focusing and plasma defocusing. Figure 5 shows the magnitudes of Δn induced in diamond by second harmonic irradiation. It is seen that, at high pulse energies, the plasma-induced polarisation exceeds the Kerr polarisation. As a result, plasma defocusing leads to rather effective light scattering in the near field, so that self-focusing cannot prevent beam divergence behind the focal plane. However, since the $\Delta n(E_s)$ curves for the Kerr effect and plasma differ markedly in the case of multiphoton absorption, they are certain to intersect as the pulse energy decreases (at E_{th} = 0.4 J cm^{-2} in our case). Under such conditions, self-focusing causes the diverging beam to converge behind the focus of the lens, shifting the plasma plume deeper into the crystal. In a certain sense, light propagation at moderate intensities will be self-matched, so that the plasma- and

Kerr effect-induced local changes in n will differ little in magnitude in the 'focusing' region (Fig. 5). At pulse powers above the critical level, self-focusing will disappear. It is easy to show that the carrier concentration will then be too low to influence electromagnetic wave propagation, and $N_e(E_s)$ will return to characteristic power law behaviour. In our experiments, such low e–h plasma densities were not detected.

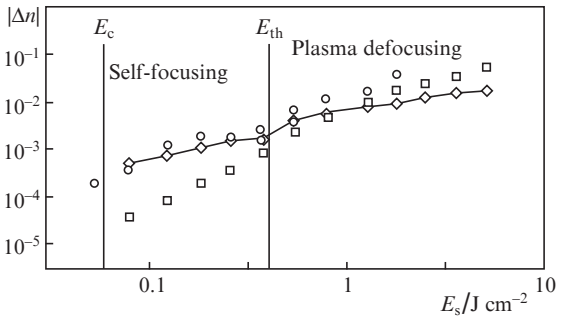

Figure 5. Comparison of the magnitudes of Δn induced by the Kerr effect (◇) and by free carrier generation in a diamond single crystal (λ = 400 nm).

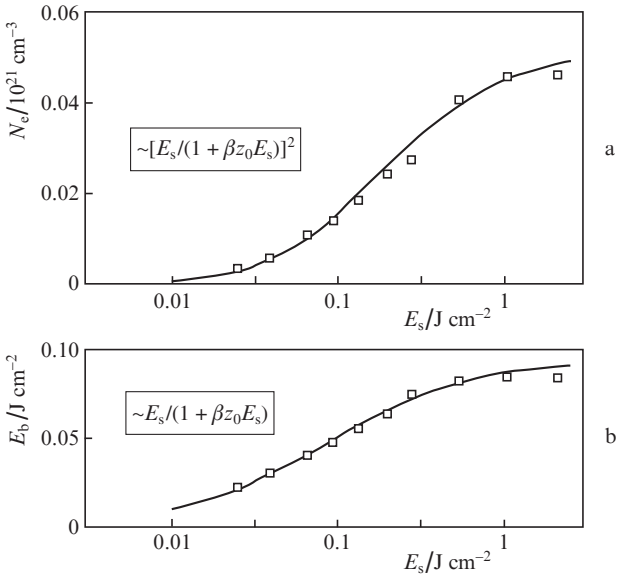

Figure 6. (a) Concentration of e–h pairs in a diamond single crystal and (b) laser fluence inside the crystal vs. laser fluence on the crystal surface (λ = 266 nm).

Clearly, the same mechanism is responsible for the nonlinear beam transformation under irradiation at λ = 800 nm, but the dispersion of the Kerr coefficient and that of the refractive index of the plasma change the thresholds for transitions between propagation regimes. As seen in Fig. 3, the complete defocusing threshold for the fundamental harmonic is $E_{th} \approx$ 4 J cm^{-2}, which exceeds the threshold at λ = 400 nm by more than ten times. Note in passing that this accounts for the experimentally observed formation of graphite filaments in the bulk of a sample when its surface is exposed to IR radiation, whereas under illumination in the visible range no such effect occurs. Indeed, at λ = 800 nm in the self-focusing regime it is easy to obtain $N_e \sim 10^{21}$ cm^{-3}, which leads to an allotropic transformation of the crystal relatively far away from the surface. At the same time, under illumination at λ = 400 nm self-focusing occurs only when N_e is reduced to $\sim 5 \times 10^{19}$ cm^{-3} (Fig. 4), which seems to be insufficient for graphitisation. As a result, raising the pulse energy leads to surface ablation, without damage in the bulk of the material.

We also obtained $N_e(E_s)$ and $E_b(E_s)$ data for the third harmonic of a Ti:sapphire laser (Fig. 6). Even though the incident power exceeded the critical power at the pulse energies used in our experiments, self-focusing proved to be even less important under femtosecond UV irradiation. In this case, beam propagation is determined primarily by two-photon absorption, which is so strong that leads to a marked reduction in intensity in the near-surface region. The effective absorption depth $(\beta_2 E_s/\tau)^{-1}$ (where τ = 120 fs is the pulse duration and β_2 is the two-photon absorption coefficient) is $\sim$100 μm at E_s = 0.01 J cm^{-2} and only $\sim$1 μm at E_s = 1 J cm^{-2}. As a result, the $E_b(E_s)$ data show nonlinear behaviour and are represented well enough by the formula $E_b = E_s/(1 + \beta_2 z_0 E_s/\tau)$, where z_0 is the pulse path length in the medium, i.e. the distance from the measurement point to the surface. This formula follows from the definition of the two-photon absorption coefficient, which can thus be estimated from the above data. The estimate thus obtained, $\beta_2 \sim 0.3 \times 10^{-9}$ cm W^{-1}, is close to values obtained by measuring transmission as a function of incident intensity: $(1-2) \times 10^{-9}$ cm W^{-1} [8, 13]. Accordingly, the e–h pair concentration in diamond under UV excitation is well represented by the formula $N_e \sim [E_s/(1 + \beta_2 z_0 E_s/\tau)]^2$ (Fig. 6a), as would be expected in the case of two-photon absorption.

This example well illustrates the above consideration that, even when a Gaussian beam is severely distorted in a sample, an interference photograph allows one to adequately establish the relationship between the state of the material and the field that induces electron transitions. Figure 7 plots the e–h pair concentration in the bulk of diamond against local laser fluence in it, $N_e(E_b)$, for the three harmonics of the Ti:sapphire laser. It is well seen that, in a wide dynamic range of laser fluences (to the point of surface and bulk graphitisation and breakdown) the absorption has a multiphoton nature. The corresponding dependences show power law behaviour with an exponent of 4 at λ = 800 nm (four-photon transition) and 2 at λ = 400 and 266 nm (indirect and direct two-photon transitions). In contrast to previous results [14], no three-photon

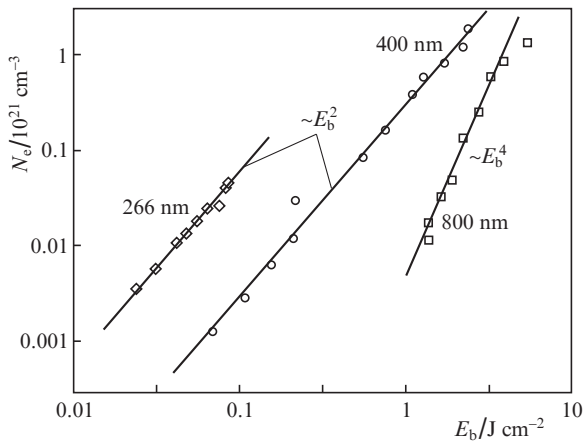

Figure 7. Concentration of e–h pairs in a diamond single crystal vs. local laser fluence.

direct transition was detected under irradiation at $\lambda = 400$ nm. Also, we did not detect any contribution of inverse bremsstrahlung to the excitation of the electron subsystem, even under irradiation at a wavelength of 800 nm.

It is worth pointing out that the above estimate of β_2 at $\lambda = 266$ nm, made essentially from optical transmission modulation measurements, can only be obtained in the case of marked pulse attenuation during propagation. If absorption is weak, as in the case of irradiation at $\lambda = 400$ and 800 nm, transmission measurements under conditions of severe beam transformation provide unreliable data. In contrast to such an approach, the $N_e = kE_b^M$ data obtained here (Fig. 7) essentially give the quantum yield of phototransitions and allow one to estimate the M photon absorption cross sections at all the wavelengths in question using the formula $\beta_M = M\hbar\omega k\tau^{M-1}$, where $\hbar\omega$ is the photon energy. The β_M values thus obtained are listed in Table 1.

Table 1. M photon absorption coefficients in diamond.

λ/nm	M	β_M
266	2	0.9×10^{-9}/cm W^{-1}
400	2	3.7×10^{-11}/cm W^{-1}
800	4	7.6×10^{-39}/cm^5 W^{-3}

4. Conclusions

Femtosecond interferometry has been used to experimentally study the photoexcitation of the electron subsystem of diamond exposed to femtosecond laser pulses at different wavelengths. The results demonstrate that, in a wide range of laser fluences (up to those resulting in surface and bulk graphitisation and breakdown), a multiphoton absorption of femtosecond radiation prevails in diamond. We have estimated nonlinear absorption coefficients at $\lambda = 800$ nm (four-photon transition) and for pulses at $\lambda = 400$ and 266 nm (indirect and direct two-photon transitions, respectively).

At the same time, it has been shown that, at any considerable path length of a femtosecond pulse in diamond (tens of microns), the laser beam experiences a severe nonlinear transformation. Together with the multiphoton absorption, this determines the local carrier concentration in the irradiated zone and the absorbed optical energy distribution. The nature of pulse propagation has been shown to be uniquely determined by the competition between wave packet self-focusing and the plasma defocusing effect. At high pulse energies, defocusing leads to effective light scattering in the near field, and the e–h plasma is concentrated in the surface layer. At moderate intensities, self-focusing begins to prevail, shifting the plasma plume deeper into the crystal. At pulse powers below the critical level, there are no nonlinear beam distortions.

When a beam is focused onto the surface of a sample, the threshold for the transition from plasma scattering to self-focusing is rather sharp, strongly depends on the incident wavelength and has a significant effect on the diamond graphitisation process.

Acknowledgements. This work was supported by the Russian Foundation for Basic Research (Grant No. 13-02-00979), the Russian Academy of Sciences (basic research programme No. PRAN 13) and the RF President's Grants Council (Support to the Leading Scientific Schools Programme, Grant No. NSh-1831.2014.2).

References

1. Allan D.C., Smith C., Borrelli N.F., Seward III T.P. *Opt. Lett*., **21** (24), 1960 (1996).
2. Schenker R.E., Oldham W.G. *J. Appl. Phys*., **82** (3), 1065 (1997).
3. Arai K., Imai H., Hosono H., Abe Y., Imagawa H. *Appl. Phys. Lett*., **53** (20), 1891 (1988).
4. Primak W., Kampwirth R. *Appl. Phys*., **39** (12), 5651 (1968).
5. Davis K.M., Miura K., Sugimoto N., Hirao K. *Opt. Lett*., **21** (21), 1729 (1996).
6. Kononenko T.V., Meier M., Komlenok M.S., Pimenov S.M., Romano V., Pashinin V.P., Konov V.I. *Appl. Phys. A: Mater. Sci. Process.*, **90** (4), 645 (2008).
7. Kononenko T., Ralchenko V., Bolshakov A., Konov V., Allegrini P., Pacilli M., Conte G., Spiriti E. *Appl. Phys. A: Mater. Sci. Process.*, **114** (2), 297 (2014).
8. Preuss S., Stuke M. *Appl. Phys. Lett*., **67** (3), 338 (1995).
9. Tallents G.J. *J. Phys. D: Appl. Phys*., **17** (4), 721 (1984).
10. Kononenko V., Pashinin V., Komlenok M., Konov V. *Laser Phys*., **19** (6), 1294 (2009).
11. Kononenko V.V., Zavedeev E.V., Latushko M.I., Pashinin V.P., Konov V.I., Dianov E.M. *Kvantovaya Elektron*., **42** (10), 925 (2012) [*Quantum Electron*., **42** (10), 925 (2012)].
12. Mildren R.P. *Intrinsic Optical Properties of Diamond* (Wiley-VCH Verlag GmbH & Co, 2013).
13. Sheik-Bahae M., DeSalvo R.J., Said A.A., Hagan D.J., Soileau M.J., Van Stryland E.W. *Proc. SPIE Int. Soc. Opt. Eng*., **2428**, 605 (1995).
14. Kozák M., Trojánek F., Dzurnák B., Malý P. *J. Opt. Soc. Am. B*, **29** (5), 1141 (2012).